Journal of Materials Chemistry C

Ferroelasticity, domain structures and phase symmetries in organic-inorganic hybrid perovskite methylammonium lead chloride

Journal:	*Journal of Materials Chemistry C*
Manuscript ID	TC-ART-04-2020-002124.R1
Article Type:	Paper
Date Submitted by the Author:	03-Jun-2020
Complete List of Authors:	Bari, Maryam; Simon Fraser University, Chemistry Bokov, Alexei; Simon Fraser University, Chemistry Ye, Zuo-Guang; Simon Fraser University, Chemistry

Ferroelasticity, domain structures and phase symmetries in organic-inorganic hybrid perovskite methylammonium lead chloride

Received 00th January 20xx,
Accepted 00th January 20xx

DOI: 10.1039/x0xx00000x

Maryam Bari♣[a], Alexei A. Bokov♣ [a]* and Zuo-Guang Ye[a]*

Hybrid organic-inorganic perovskites $CH_3NH_3PbX_3$ (X=I, Cl and Br) have recently been developed as highly efficient materials for optoelectronic applications. However, the mechanisms of their extraordinary performance remain poorly understood. It has been suggested that ferroelectric domains may be responsible for photovoltaic behavior of hybrid perovskites employed in solar cells, but the very existence of ferroelectricity in these materials remains debatable. Furthermore, due to the presence of disordered organic group, the hybrid crystal structure is difficult to determine by conventional diffraction methods and controversial results have been reported. In this work $CH_3NH_3PbCl_3$ crystals are investigated using polarized light microscopy in the temperature range from 80 to 400 K. It is found that symmetry of the phase appearing after the high-temperature cubic phase upon cooling is orthorhombic but not tetragonal, as believed before. It transforms into another orthorhombic phase at a lower temperature. In both orthorhombic phases twin domains are found and examined under mechanical stress and electric field. The crystal proved to be ferroelastic but not ferroelectric.

Introduction

Tremendous progress has been achieved in the technology of photovoltaic power conversion devices based on organic-inorganic hybrid lead halide perovskites during the past ten years.[1-6] However, the nature of the observed extraordinary properties remains debatable. One of the main reasons why the behavior of hybrid perovskites is hard to interpret is the complexity of their crystal structure. Besides heavy metal ions, it contains comparatively light polar molecular cations whose orientation is difficult to determine using traditional diffraction techniques. Meanwhile, the orientation of organic molecules affects the crystal symmetry and has been found to play an essential role in determining the electronic properties responsible for slow carrier recombination and the superior energy conversion efficiency.[7] Of particular interest in this respect is the ongoing discussion on the ferroelectricity in methylammonium (MA) halide perovskites, $MAPbX_3$, which may possibly result from the ordering of polar organic molecules.[5] Some researchers[8] reported ferroelectric properties in $MAPbI_3$, while some others did not confirm these properties.[9-12] Domain structures were observed near the surface of $MAPbI_3$ samples using piezoresponse force microscopy (PFM),[13-15] transmission electron microscopy[16] and optical microscopy in reflected light.[17] Those domains were postulated to be ferroelectric, [13-15] or argued to be ferroelastic, but not ferroelectric.[17] It was recently concluded, that the ferroelectric-like behavior of domains observed in $MAPbI_3$ by PFM originates from experimental artefacts,[18,19] but this conclusion has been challenged.[20]

According to early X-ray diffraction investigations,[6] the temperature-driven sequence of phases in all $MAPbX_3$ compounds is similar: the high-temperature phase (α phase) is of cubic perovskite structure (C) with space group $Pm\bar{3}m$, the low-temperature phase is orthorhombic (O), and a tetragonal (T) structure is located in the temperature interval between the C and O phases. This behavior has been confirmed in many X-ray and neutron diffraction experiments,[4,6,21,22] but space groups assigned to the phases have been the subject of controversy. In particular, in the intermediate phase (β phase) of $MAPbI_3$ different authors revealed polar *I4cm* space group[23,24] which allows ferroelectricity or *I4/mcm* group[6,9,25,26] for which ferroelectricity is impossible. Furthermore, recent diffraction studies have suggested that the low-temperature (γ) phase of $MAPbI_3$ adopts a monoclinic (M) rather than O crystal system[23] and α phase is tetragonal[23,27] or rhombohedral[27] with a very small distortion of cubic perovskite cell overlooked in earlier investigations. However, the authors were unable to refine the crystal class of M phase because the studied crystals were heavily twinned. Similar problems arose for $MAPbCl_3$, where recent studies of the α phase revealed a subtle deviation of the observed X-ray diffraction pattern from that predicted for the cubic symmetry and the neutron diffraction features indicating possible ferroelectric-type displacements of Pb ions.[27] It was suggested that synchrotron structural investigations are needed to get unambiguous conclusions. In the β phase of $MAPbCl_3$ the tetragonal space group *P4/mmm* was initially reported,[6] however, subsequent diffraction investigations of single crystals[21] revealed the superstructure reflections of two types, corresponding to cell doubling and about threefold incommensurate modulation, respectively, along the *c*-axis. It was concluded that the crystal system seems to be tetragonal

a Department of Chemistry and 4D LABS, Simon Fraser University, Burnaby, British Columbia, V5A 1S6, Canada
♣These authors contributed equally to this work.
*Corresponding Authors' E-mails: abokov@sfu.ca and zye@sfu.ca
Electronic Supplementary Information (ESI) available: [details of any supplementary information available should be included here]. See DOI: 10.1039/x0xx00000x

with the unit cell containing four formula-units. However, it was difficult to analyze the structure because of significant twinning, and the space group was not assigned. For the low-temperature γ phase of $MAPbCl_3$ the orthorhombic space group $P222_1$ was initially found with perovskite cell doubling along the [001] direction.[6] Later neutron and synchrotron x-ray diffraction experiments revealed the space group $P2_12_12_1$[21]or *Pnma*[22] with cell doubling along all three orthorhombic <100> directions.

We investigate here the $MAPbCl_3$ crystals by means of optical crystallography, which is known to allow a more accurate determination of the crystal system than diffraction crystallography.[28] In contrast to diffraction methods where twin domains complicate the refinement of the crystal structure, optical crystallography employs the domain morphology as a convenient and powerful research tool to resolve the domain structure and phase symmetry. In contrast to previous investigations of domain structure, which has been performed at room temperature in the tetragonal phase of another hybrid lead halide perovskite, $MAPbI_3$, by the methods which only probe the near-surface regions of a crystal (electron microscopy, piezoresponse force microscopy, reflection optical microscopy) we applied transmission polarized light microscopy (PLM), which allows bulk observations at a wide temperature range in different phases.

Results and discussion

Transparent, colorless, rectangular cuboid shaped $MAPbCl_3$ single crystals were grown from solution. Fig. 1(a) demonstrates that X-ray diffraction at room temperature yields a cubic perovskite structure with the space group $Pm\overline{3}m$ and lattice parameter a = 5.684 Å consistent with the previous reports.[6,21,27] The temperature dependence of permittivity shown in Fig. 1(b) is similar to that observed in the MAPbCl3 crystals previously. [11] Two sharp jumps at 178 and 172 K are related to the transitions from α to β and from β to γ phases, respectively. Upon heating to about 600 K, the crystals became less transparent irreversibly, which indicates the onset of decomposition, consistent with our differential scanning calorimetry (DSC) analysis and the thermal analysis reported previously.[29]

Crystal symmetry can be determined by analyzing the positions at which the crystal appears in extinction under polarized light microscope. For ferroelastics and ferroelectrics an additional information can be obtained from the orientation of domain walls as described in Supporting Information Section 1 and in Table 1. We find that in the α phase the crystals remain in extinction at any observation direction and any position between crossed polarizers (see Supporting Information Section 2), which means that the birefringence is absent, and the symmetry is cubic. Linear birefringence (Δn) appears after cooling the crystal below the temperature of 178 K, i.e. in the β and γ phases. Twin domain structure is often observed in these phases, while single domain crystals can also be obtained. The examples are presented in Fig. 2 and in Supporting Information Sections 3 and 4. Different configurations of domains were observed in different specimens and in the same specimen after several cooling-heating runs through phase transitions, but when the temperature varies within the same phase, the domain structure remains unchanged. Such a behavior is typical of ferroelastic (and ferroelectric) crystals.

Fig. 1(c) shows the temperature dependences of Δn measured on (001) crystal plates, i.e. the plates having large surfaces parallel to one of the {100} crystallographic planes, so that the observation is performed along the <001> direction (throughout the article we refer to the crystallographic axes of the parent cubic phase). Abrupt variations of birefringence are observed at the α-β and β-γ phase transitions with temperature hysteresis between cooling and heating runs of 0.9 K and 1.1 K, respectively. The discontinued changes and the thermal hysteresis unambiguously suggest that both transitions are of the first order.

The domain structure typical of the β phase in large crystals is demonstrated in Fig. 2(a). The domain walls are visible in the form of lines extending along [100] and [010], i. e. the intersections of walls with the crystal surface form angles of $\varphi = 0^o$ or $\varphi = 90^o$ to the <100> directions, which is possible in any phase, according to Table 1. The distance between the parallel walls (domain thickness) is 4-20 μm. In some regions a cross-hatched microstructure ('tweed pattern') and comb pattern at the intersection of two bundles of mutually perpendicular domain strips are observed. Such motifs are characteristic of ferroelastic domains.[30]

Another example of domain structure in the β phase is shown in Fig. 2(b) and (c). Two large domains are visible with complete extinctions at $\delta = 0^o$ and $\delta = 45^o$, respectively. According to Table 1, only in orthorhombic O_S phase such two extinction positions are possible simultaneously (O_S stands for the ferroelastic orthorhombic phase in which one of the twofold symmetry axes is along the face diagonal of the parent cubic cell; see Supporting Information Section 1 for details). Note also different colors of these domains and the region between the domains which reveals parallel bands of alternating colors with a sequence that matches the sequence of low-order interference colors in the Michel-Levi chart.[28] This multicolor region is due to the wedges formed by the inclined domain wall and the surfaces of the crystal plate, as schematically demonstrated in Fig. 2(d). The angle φ is found to be 34°. The walls having an angle φ other than 0°, 45° or 90° are called S-walls. According to Table 1, they are not possible in T phase, but allowed in the O_S phase.

One can determine from the Michel-Levi chart that the color of the lower domain corresponds to the second-order yellowish green interference color which is produced by optical retardation of $\Delta \approx 880$ nm. The value of $\Delta \approx 300$ nm corresponds to the first-order yellow of the upper domain. The effective birefringence calculated as $\Delta n = \Delta/t$ (where t = 0.13 mm is the crystal thickness) appears to be $\Delta n_1 = 0.007$ and $\Delta n_2 = 0.002$ for lower and upper domains, respectively, in agreement with the values reported in Fig. 1(c).

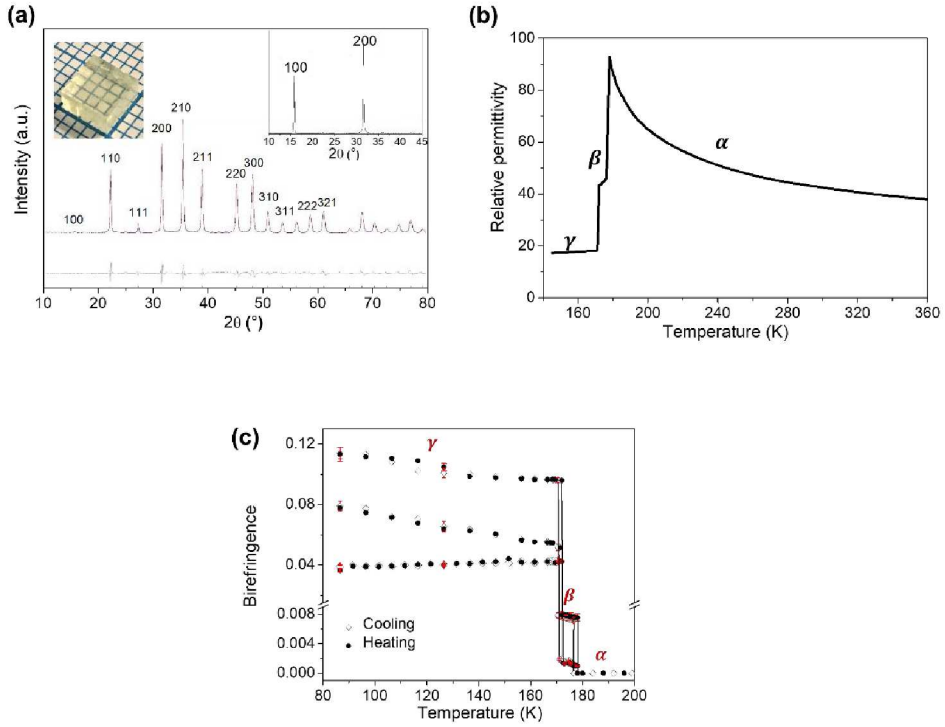

Fig. 1 Structural, dielectric, and optical characterizations of $CH_3NH_3PbCl_3$ crystals. (a) Powder X-ray diffraction pattern obtained at room temperature from ground crystals (black line), the result of refinement with the profile residual factor R_{wp} =2.01 (red line) and the difference (line at the bottom of the panel). The inset shows the pattern obtained from the crystal surface, confirming that the grown facets are the {100} crystallographic planes. (b) Temperature dependence of the relative permittivity measured on heating at the frequency of 100 kHz. (c) Temperature dependence of linear birefringence (Δn) measured on (001) oriented crystals on cooling and heating. Distinct Δn values at the same temperature in the β and γ phases correspond to different orientation states (domains). In γ phase these are three principal birefringences. Error bars are calculated from measurements in three or more different crystals.

Tetragonal and rhombohedral crystals are uniaxial, and all domains of these crystals should have the same effective birefringence when observed in (001) plate. In contrast, different sections of the optical indicatrix can be seen under the microscope in different domains of biaxial orthorhombic crystals and the values of Δn can be different. Therefore, the extinction positions, the domain wall directions and different birefringence values in different domains indicate that the β phase of $MAPbCl_3$ crystal is not tetragonal, as previously believed based on diffraction data, and the only phase compatible with the crystal optical characteristics observed by PLM is the orthorhombic O_S.

From the wall angle φ = 34° the monoclinic angle of distorted primitive cell can be calculated. The orientations of S-walls are related to lattice parameters through the relative spontaneous strain tensor. For the orientation state of O_S phase in which the b axis is parallel to the x axis of the orthogonal x, y, z system (i. e. for the upper domain in Fig. 2(d)), this tensor can be written as.[30]

$$\begin{pmatrix} 0 & 0 & 0 \\ 0 & S & R \\ 0 & R & S \end{pmatrix} \quad (1)$$

The components are defined as $S = (a - b)(2a + b)^{-1}$ and $2R = 0.5\pi - \beta$, where a, b and β are the parameters of the monoclinically distorted primitive cell. The equation of the S-wall between two orientation states depicted in Figure 2d is given as follows: [31]

$$3S(x - z) = 2Ry \quad (2)$$

The angle φ can be determined from this equation through the relation $3S\cot\varphi=2R$ and the monoclinic angle can be found as:

$$\beta = \frac{\pi}{2} - 3\frac{a-b}{2a+b}\cot\varphi \quad (3)$$

Considering the reported[21] lattice parameters of pseudotetragonal superstructure: a_T = 11.290(16) Å, b_T = 11.290(4) Å and c_T = 11.303(9) Å and making an evident choice of $a = 0.5a_T$, and $b = 0.5c_T$, we find from the last equation that β = 90°6′. Such a small deviation from the right angle had been overlooked in x-ray and neutron diffraction experiments and analysis and therefore, the tetragonal system was erroneously assigned. Taking into account the necessary doubling of lattice parameters due to superstructure (which cannot be verified by means of PLM), the parameters of the conventional orthorhombic cell can be estimated as $a_O = 2a\sqrt{2 - 2\cos\beta}$ = 15.980 Å, $b_O = 2a\sqrt{2 + 2\cos\beta}$ = 15.953 Å, and c_O = 2b = 11.303 Å. Note that the difference $a_O - b_O$ = 0.027 Å is very small and equals approximately the uncertainty of lattice parameter determination in the diffraction experiments[21] and that the possible incommensurate structural modulation

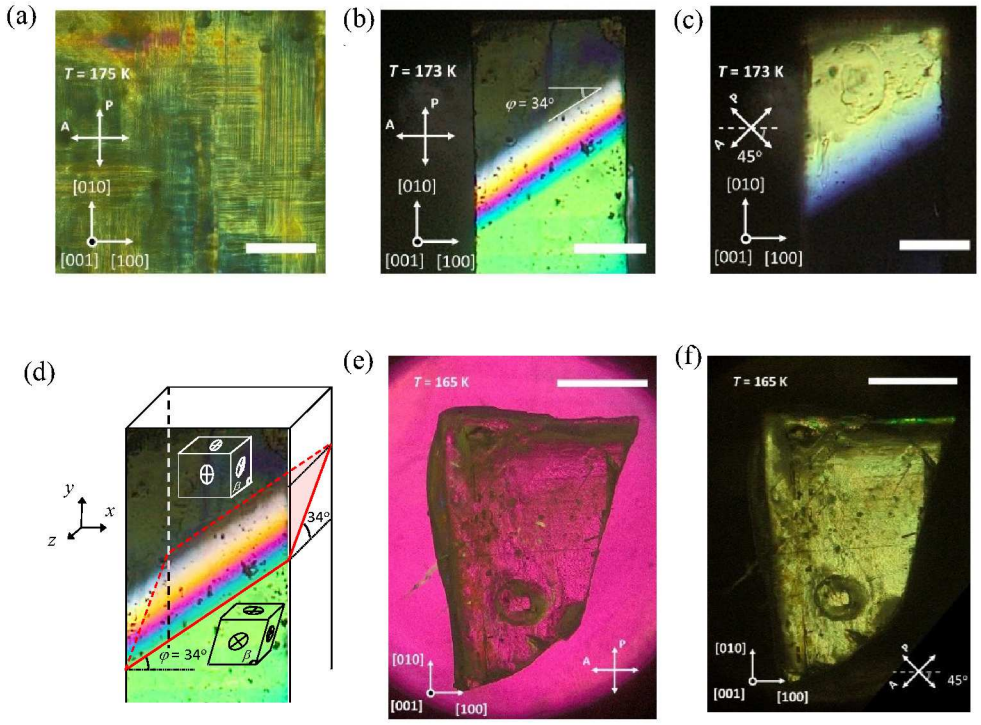

Fig. 1 Examples of domain structure observed with polarizing microscope on (001) oriented $CH_3NH_3PbCl_3$ crystal plates. (a) Complex domain structure of the β phase in a part of a large crystal which has been polished down to a thickness of t ≈ 0.2 mm. A quarter wavelength plate is superimposed to improve the visibility of domains. (b) and (c) Two domains in the β phase of a small crystal with as-grown faces and t = 0.13 mm. (d) Schematics of domain configuration in the crystal depicted in b and c. The S-wall is highlighted by red and the monoclinically distorted primitive cells in two adjacent domains are shown. (e) and (f) The same crystal as in a after cooling into the γ phase. A first-order red plate is superimposed in (f) to distinguish the non-transparent regions (black) and the regions in complete extinction (magenta). No domain walls can be found, and the orientation of the indicatrix axes (determined by a compensator) is the same in all areas, which indicates that the crystal consists of a single ferroelastic domain. The temperature, the directions of crystallographic axes, indicatrix axes and polarizers and the angle δ = 0o (b) and (f) and δ = 45o (c) and (e) between the polarizers and [100] are indicated. Scale bars are 100 μm (a-c) and 500 μm (e) and (f).

reported in the β phase with X-ray diffraction[21] is not accessible in the PLM observations.

Domains in the γ phase are usually larger than in the β phase, and single-domain states are often observed even in comparatively large specimens, such as the crystal shown in Fig. 2(e) and (f). The complete extinction is observed in this crystal at $\delta = 0^0/90^\circ$, as expected (see Table 1) in all orientation states of O_P phase and in some orientation states of T, O_S and M_C phases (O_P stands for the ferroelastic orthorhombic phase in which all twofold symmetry axes are along one of the crystallographic axes of the parent C phase; for the definition of M_C phase, see Methods). However, the uniaxial T phase should be excluded because the domains with three different Δn were found in the (001) plates (see Fig. 1(c)). Furthermore, in all these domains the extinction at $\delta = 0^0/90^\circ$ is found, which excludes the M_C phase. We conclude, therefore, that the γ phase has the O_P structure, which is in agreement with the previous diffraction studies.[4,6,21]

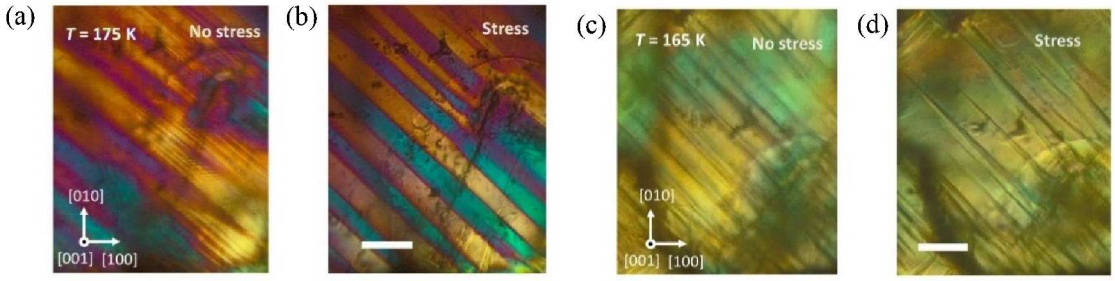

Fig. 2 Verification of ferroelastic nature of twin domains observed on $CH_3NH_3PbCl_3$ crystals. (a-d), Photographs of (001) plate under polarizing microscope in the β phase (a) and (b) and γ phase (c) and (d); with a uniaxial stress applied along [001] (b) and (d) and without stress (a) and (c). A first-order red plate is superimposed to improve the visibility of domains. Plate thickness = 0.25 mm; scale bars = 100 μ m.

Table 1 Permissible extinction directions and orientations of ferroelastic domain walls which can be observed by polarizing microscope in the (001) crystal plate after transformation from the cubic prototype $m\bar{3}m$ phase to ferroelastic phases of different symmetries: rhombohedral (R), tetragonal (T), orthorhombic (O_P and O_S), (monoclinic M_A, M_B and M_C) and triclinic (Tr). δ is the angle between the crossed polarizers and the <100> directions at which the extinction is observed; the filled circle (•) indicates that domains which are in extinction at any δ angle are possible; the crossed circle (⊕) indicates that regions without extinction at any δ are possible; φ is the permissible angle between a domain wall trace on the crystal surface and the <100> direction (walls which are *not* perpendicular to a crystal surface are listed in brackets); angles $\varphi = \varphi_i$ and $\delta = \delta_i$ (i=1, 2, …) may adopt any value, except 0° , 90° and ± 45°.

Phase	Angles	
	δ	φ
T	0°,90°, •	(0°,90°), ±45°
R	±45°	0°,90°, (0°,90°), ±45°
O_P	0°,90°	(0°,90°), ±45°
O_S	0°,90°, ±45°, ⊕	0°,90°, (0°,90°), ±45°, (±45°), (±φ_1), (90°±φ_1)
M_A, M_B	±45°, ±45°±δ_1, ⊕	0°,90°, (0°,90°), ±45°, (±45°), (±φ_1), (90°±φ_1)
M_C	0°,90°, 0°,90° ±δ_1, ⊕	0°,90°, (0°,90°), ±45°, (±45°), (±φ_1), (90°±φ_1)
Tr	±45°±δ_i (i=1,2,3), ⊕	0°,90°, (0°,90°), ±45°, (±45°), (±φ_i), (90°±φ_i)

Ferroelastics are defined as crystals in which an external stress can transform ("switch") one crystallographic orientation (spontaneous strain) state into another. In practice the transformation occurs via the displacement of walls separating ferroelastic domains. The wall displacement implies that the near-wall regions are switched. Therefore, to prove the ferroelastic nature of twin domains, a significant stress-induced rearrangement of domain structure should be demonstrated. Uniaxial stress was applied in our experiments in the direction perpendicular to the major crystal face (i. e. parallel to the optical axis of the microscope). Fig. 3(a-d) shows that in the β and γ phases an external stress changes the domain structure, confirming that both phases are ferroelastic.

In ferroelectric perovskite crystals two types of ferroelectric domains can be expected: 180° domains (which are non-ferroelastic) and non-180° domains (which always reside with ferroelastic twin domains due to coupling between lattice polarization and strain). If a crystal is not only ferroelastic, but also ferroelectric, all domains should be switchable by an external electric field (by the definition of ferroelectricity). In our experiments a field of up to 15 kV/cm was applied. When a comparatively large field was applied for a long time (several minutes), the specimen became less transparent, but the birefringence did not change, and no variations of domain wall positions were noticed. This behaviour is evidenced in Fig. 4, which demonstrates that in both the β and γ phases the domain structure before [Fig. 4(a) and (c)] and after [Fig. 4(b) and (d)] application of electric field is exactly the same. Therefore, $MAPbCl_3$ is not ferroelectric and the observed domains are ferroelastic twins.

An additional test for ferroelectricity consists in the measurements of phase transition temperatures under electric field. They were determined as the temperatures where the domain structure changes on heating or cooling. The temperature of transition from ferro- to paraelectric phase should increase under external electric field and the transition temperature between two ferroelectric phases also may change. However, the transition temperatures are found to be independent of the applied electric field (see Fig. S6), which confirms that $MAPbCl_3$ is not ferroelectric.

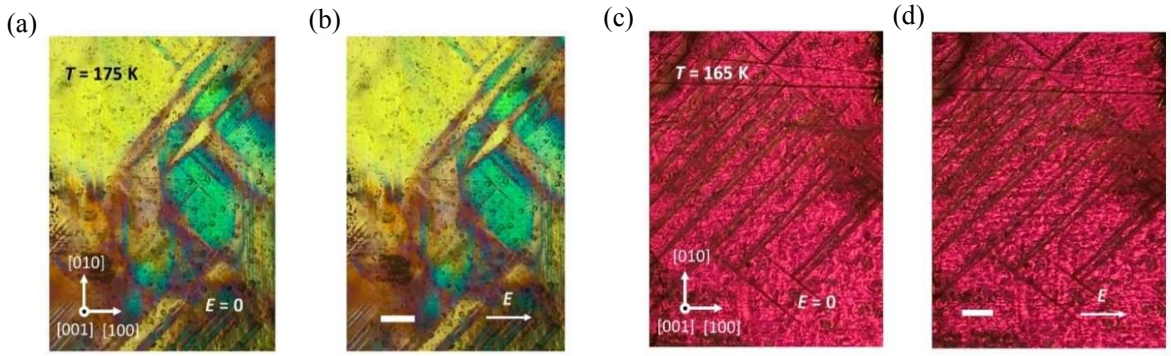

Fig. 3 Verification of ferroelectric nature of domains observed on CH3NH3PbCl3 crystals. (a-d), Photographs of (001) plate under polarizing microscope in the β phase (a) and (b) and γ phase (c) and (d); without electric field (a) and (c) and with an electric field of 15 kV/cm applied along [010] (b) and (d). A first-order red plate is superimposed to improve the visibility of domains. Crystal thickness = 0.2 mm; scale bars = 100 μ m.

Experimental

Growth of $CH_3NH_3PbCl_3$ crystals

Two salts, CH_3NH_3Cl and $PbCl_2$, were first dissolved into DMSO by stirring at 60 °C for 2 hours to obtain a 2[M] homogenous solution. After that, the solution was cooled down to 25 °C and kept at room temperature for several days. Highly transparent, colourless crystals were grown with well-defined rectangular habits compatible with the cubic symmetry with the dimensions from several micrometres to several millimetres, depending on the crystal growth time.

Powder X-ray diffraction

Crystal structure and phase purity were verified by a Rigaku Rapid Axis Diffractometer using Cu *Kα* radiation in the Bragg-Brentano reflection geometry. Structural refinement was performed by the Pawley method using TOPAS software package.

Polarized light microscopy (PLM)

Crystals of various sizes were selected for examination, including thin (~ 0.1 mm) plates and larger specimens. The crystallographic orientation of the crystals was confirmed using specular diffraction from the surface of crystals, as shown in the inset of Figure 1(a), which is consistent with the rectangular morphology of the $\{100\}_{cub}$ as-grown faces. To prepare thin platelets with large faces parallel to (001), (011) and (111) crystallographic planes, respectively, suitable for optical examination, large crystals were thinned and mirror polished; as-grown (001) plates were also studied provided they were thin enough. An Olympus BX60 polarizing microscope equipped with a first order red plate (530 nm), a quarter wavelength retardation plate (137 nm) and a Linkam HTMS600 heating/cooling stage was used for investigations in the temperature range of 80 - 400 K. Birefringence was measured using Berek compensators of Olympus U-CBE and U-CTB. Single-domain crystals or large domains in poly-domain crystals were selected for measurements that were carried out at temperatures stabilized in the course of slow (~ 1 K min^{-1}) heating and cooling. To apply uniaxial stress the crystal was placed between two quartz coverslips and the top coverslip was pressed. To apply an electric field two parallel stripes of gold were deposited on one of the large (001) faces of the crystal plate by sputtering. The stripes were used as electrodes being connected to a high voltage source by gold wires.

Dielectric measurements

The dielectric permittivity was measured using an impedance analyzer (Novocontrol Turnkey Dielectric Spectrometer, Concept 40) at a measurement frequency of 100 kHz and a field strength of about 5 V mm^{-1}. Opposite (100) faces of the crystal plate were covered with silver paste to form electrodes which were connected to the spectrometer by gold wires. The data were collected upon heating at the rate of 0.5 K min^{-1}.

Conclusions

In summary, we perform a comprehensive study of hybrid perovskite crystals by means of polarized light microscopy, which examine not only near-surface regions, like other techniques previously used to investigate the domain structure in $MAPbI_3$, but also the bulk properties of the crystals. We find ferroelastic twin domains in $MAPbCl_3$ and show unambiguously that this material is not ferroelectric. This suggests that even if ferroelectricity really existed in other hybrid lead halide perovskites, it might not play a major role in the appearance of their extraordinary optoelectronic properties. We also resolve the ambiguity regarding the crystal structure of $MAPbCl_3$ and find that the intermediate phase that was postulated to be tetragonal is of orthorhombic symmetry. Upon cooling the crystal transforms from the cubic α phase, to orthorhombic (O_S) β phase and then to the orthorhombic (O_P) γ phase. The domain structure of the orthorhombic β phase is characterized by the presence of *S*-wall. This finding will be helpful in determining more accurately the arrangement of methylammonium molecules in the halide perovskite crystal structure, which is inaccessible by diffraction methods, but is of relevance to the macroscopic symmetry and crystal physical properties.

Conflicts of interest

There are no conflicts to declare.

Acknowledgements

This research was supported by the Natural Sciences and Engineering Research Council of Canada (NSERC, Grant No. 203773) and the U. S. Office of Naval Research (Grant No. N00014-16-1-3106).

Notes and references

1 M. Lee, J. Teuscher, T. Miyasaka, T. Murakami and H. J. Snaith, *Science*, 2012, **338**, 643-647.
2 J. Burschka, P. Norman, S. J Moon, R. Humphry-Baker, P. Gao, M. K. Nazeeruddin and M. Grätzel, *Nature*, 2013, **499**, 316-319.
3 M. U. Rothmann, W. Li, J. Etheridge and Y.-B. Cheng, *Adv. Energy Mater.*, 2017, **7**, 1700912.
4 Q. Chen, N. De MarcO, Y. Yang, T-B Song, C. C. Chen, H. Zhao, Z. Hong, H. Zhou and Y. Yang, *Nano Today*, 2015, **10**, 355-396.

5 J. M. Frost, K. T. Butler, F. Brivio, C. H. Hendon, M. Schilfgaarde and A. Walsh, *Nano Lett.*, 2014, **14**, 2584-2590.
6 A. Poglitsch and D. Weber, *J. Chem. Phys.*, 1987, **87**, 6373-6378.
7 C. Motta, F. El-Mellouhi, S. Kais, N. Tabet, F. Alharbi and S. Sanvito, *Nat. Commun.*, 2015, **6**, 7026.
8 Y. Rakitaa, O. Bar-Ellib, E. Meirzadeha, H. Kaslasia, Y. Pelega, G. Hodesa, I. Lubomirskya, D. Oronb, D. Ehrea and D. Cahena, *Proc. Natl. Acad. Sci. U. S. A.*, 2017, **114**, 5504-5512.
9 G. Sharada, P. Mahale, B. P. Kore, S. Mukherjee, M. S. Pavan, C. De, S. Ghara, A. Sundaresan, A. Pandey, T. N. Guru Row and D. D. Sarma, *J. Phys. Chem. Lett.*, 2016, **7**, 2412-2419.
10 Z. Xiao, Y. Yuan, Y. Shao, Q. Wang, Q. Dong, C. Bi, P. Sharma, A. Gruverman and J. Huang, *Nat. Mater.*, 2015, **14**, 193-198.
11 I. Anusca, S. Balčiūnas, P. Gemeiner, Š. Svirskas, M. Sanlialp, G. Lackner, C. Fettkenhauer, J. Belovickis, V. Samulionis, M. Ivanov, B. Dkhil, J. Banys, V. V. Shvartsman and D. C. Lupascu, *Adv. Energy Mater.*, 2017, **7**, 1700600.
12 M. N. F. Hoque, M. Yang, Z. Li, N. Islam, X. Pan, K. Zhu and Z. Fan, *ACS Energy Lett.*, 2016, **1**, 142-149.
13 Y. Kutes, L. Ye, Y. Zhou, S. Pang, B. D. Huey and N. P. Padture, *J. Phys. Chem. Lett.*, 2014, **5**, 3335-3339.
14 B. Chen, X. Zheng, M. Yang, Y. Zhou, S. Kundu, J. Shi, K. Zhu and S. Priya, Nano Energy., 2015, **13**, 582-591.
15 H. Röhm, T. Leonhard, M. J. Hoffmann and A. Colsmann, *Energy Environ. Sci.*, 2017, **10**, 950-955.
16 M. U. Rothmann, W. Li, Y. Zhu, U. Bach, L. Spiccia, J. Etheridge and Y. B. Cheng, *Nat. Commun.*, 2017, **8**, 14547.
17 E. Strelcov, Q. Dong, T. Li, J. Chae, Y. Shao, Y. Deng, A. Gruverman, J. Huang and A. Centrone, *Sci. Adv.*, 2017, **3**, 1602165.
18 Y. Liu, L. Collins, R. Proksch, S. Kim, B. R. Watson, B. Doughty, T. R. Calhoun, M. Ahmadi, A. V. Ievlev, S. Jesse, S. T. Retterer, A. Belianinov, K. Xiao, J. Huang, B. G. Sumpter, S. V. Kalinin, B. Hu and O. S. Ovchinnikova, *Nat. Mater.*, 2019, **18**, 1051-1053.
19 A. Gómez, Q. Wang, A. R. Goñi, M. Campoy-Quiles and A. Abate, *Energy Environ. Sci.*, 2019, **12**, 2537-2547.
20 . D. Schulz, H. Rohm, T. Leonhard, S. Wagner, M. J. Hoffmann and A. Colsmann, *Nat. Mater.*, 2019, **18**, 1050.
21 Y. Kawamura and H. Mashiyama, *J. Korean Phys. Soc.*, 1999, **35**, 1437-1440.
22 L. Chi, I. Swainson, L. Cranswick, J.-H. Her, P. Stephens and O. Knop, *J. Solid State Chem.*, 2005, **178**, 1376-1385.
23 C. C. Stoumpos, C. D. Malliakas and M. G. Kanatzidis, *Inorg. Chem.*, 2013, **52**, 9019-9038.
24 Y. Dang, Y. Liu, Y. Sun, D. Yuan, X. Liu, W. Lu, G. Liu, H. Xia and X. Tao, *CrystEngComm*, 2015, **17**, 665-670.
25 T. Baikie, Y. Fang, J. M. Kadro, M. Schreyer, F. Wei, S. G. Mhaisalkar, M. Graetzel and T. J. White, *J. Mater. Chem. A*, 2013, **1**, 5628-5641.
26 M. T. Weller, O. J. Weber, P. F. Henry, A. M. Di Pumpo and T. C. Hansen, *Chem Commun*, 2015, **51**, 4180-4183.
27 T. Baikie, N. S. Barrow, Y. Fang, P. J. Keenan, P. R. Slater, R. O. Piltz, M. Gutmann, S. G. Mhaisalkar and T. J. White, *J. Mater. Chem. A*, 2015, **3**, 9298-9307.
28 F. D. Bloss, An Introduction to the Methods of Optical Crystallography, Holt, Rinehart and Winston, New York, 1961.
29 B. Brunetti, C. Cavallo, A. Ciccioli, G. Gigli and A. Latini, *Sci. Rep.*, 2016, **6**, 31896.
30 E. K. H. Salje, *Annu. Rev. Mater. Res.*, 2012, **42**, 265-283.
31 J. Sapriel, *Phys. Rev. B*, 1975, **12**, 5128-5140.